PTEP

Prog. Theor. Exp. Phys. **2016**, 073B10 (12 pages)
DOI: 10.1093/ptep/ptw097

The Yang–Mills gradient flow and lattice effective action

Ryo Yamamura*

Department of Physics, Osaka University, Toyonaka, Osaka 560-0043, Japan
*E-mail: ryamamura@het.phys.sci.osaka-u.ac.jp

Received June 8, 2016; Accepted June 9, 2016; Published July 27, 2016

Recently, the Yang–Mills gradient flow has been found to be a useful concept not only in lattice simulations but also in continuous field theories. Since its smearing property is similar to the Wilsonian "block spin transformation", there might be a deeper connection between them. In this work, we define the "effective action", which generates configurations at a finite flow time, and derive the exact differential equation to investigate the flow-time dependence of the action. Then the Yang–Mills gradient flow can be regarded as the flow of the effective action. We also propose a flow-time-dependent gradient, where the differential equation becomes similar to the renormalization group equation. We discuss the possibility of regarding the time evolution of the effective action as the Wilsonian renormalization group flow.

Subject Index B01, B38

1. Introduction

Recently, the Yang–Mills gradient flow (or the Wilson flow) [1–4] has been found to be a useful concept in lattice simulations and has been widely applied to various issues. Since it is regarded as a continuous stout smearing of the link variables, effects coming from the lattice cutoff are reduced while the IR (or long-range) physics is kept unchanged. Moreover, the fact that the smeared link variables look similar to the smooth renormalized fields enables us to measure the topological charge and energy–momentum tensor even on the lattice.

The gradient flow shows attractive properties not only in lattice simulations but also in continuous field theories. In the 4D pure Yang–Mills theory, any correlation function in terms of the gauge fields at a finite flow time ($= t$) is finite without additional renormalization, once the gauge coupling is renormalized suitably [5]. The 2D $O(N)$ nonlinear sigma model has also been studied and its renormalizability shown [6,7].

Since the smearing property of the gradient flow is similar to the Wilsonian "block spin transformation", we want to reveal a deeper relation between them, or eventually construct the Wilsonian renormalization group (RG) using the good properties of the gradient flow. One of the advantages of this approach is that the gradient flow is compatible with the gauge symmetry. Thus there is the possibility of carrying out a Wilsonian RG transformation in a gauge-symmetric way, which is usually difficult in functional RG approaches with a momentum cutoff.

As a first step towards achieving the above final goal, it could be worth studying the "effective action" of the 4D lattice $SU(3)$ pure Yang–Mills theory, which generates configurations smeared by

Funded by SCOAP^3

the Wilson flow. This effective action is defined by changing the integration variables,

$$e^{-S_t[V]} \equiv \int DU\ \delta(V - \bar{V}_t[U])\ e^{-S_{\mathrm{W}}[U]}, \tag{1}$$

where S_{W} is the Wilson plaquette action and $\bar{V}_t[U]$ is the solution of the Wilson flow equation with the initial condition $\bar{V}_0[U] = U$.

In our previous work [8], the t dependence of S_t has been investigated by the lattice simulation. S_t is truncated so that it contains Wilson plaquettes and rectangles only and their corresponding couplings are determined by the demon method [9,10]. The result shows that the coupling of the plaquette grows while that of the rectangle tends to become negative with increasing flow time, like the known improved actions [11–16]. However, the obtained trajectory in 2-coupling theory space travels in the opposite direction to the renormalization trajectory investigated by the QCD-TARO collaboration [16]. In Fig. 1 of Ref. [16], the coefficients of the plaquette (β_{11}) and the rectangle (β_{12}) finally go towards the origin after RG transformation. On the other hand, Fig. 3 of Ref. [8] shows that their absolute values (β_{plaq} and β_{rect}) monotonically grow with increasing flow time and the trajectory goes away from the origin.

In this work, we propose a different method to study the effective action. We derive the exact differential equation for S_t starting from the Wilson flow equation for the link variables. The solution of this proposed equation tells us the t dependence of couplings. Unlike previous work, we do not need to implement lattice simulations in our method. As an application, we give a solution in a truncated 8-coupling theory space. Note that the truncation of the action is just for a practical reason and our differential equation itself is exact without any truncation. In the Wilsonian RG, the flow of the Wilsonian effective action is always discussed. Our differential equation enables us to regard the gradient flow as the flow of the effective action. This could be a new notion of gradient flow, which has been regarded as the relation between the configurations only. We discuss two types of gradient flow.

We first discuss the Wilson flow as a continuation of our previous work [8]. In this case, the differential equation is just a linear inhomogeneous first-order differential equation and its solution can be obtained analytically. The result agrees with that of Ref. [8] on the negativeness of the coupling of the rectangle. On the other hand, the coupling of the plaquette shows different behavior. In contrast to the monotonic increase observed in Ref. [8], it increases in the small-t region and tends to decrease at around $\sqrt{8t} \simeq 1$ in our result. We find that this difference can be understood as the difference of the truncation.

We then propose an extension of the differential equation to more generic cases: it is not limited to the Wilson flow but can take any t-dependent lattice action for the gradient flow equation. For example, the "trivializing action" [2], which gives a vanishing S_t at a fixed $t = t_0$, could be a good candidate. In this work, S_t itself is taken as a concrete example of the t-dependent action, where the extended differential equation is quadratic in S_t and becomes similar to the RG equation. In this sense, this extended flow looks more similar to the unknown RG equation than the previous case. We also give a solution in the same truncated theory space as the case of the Wilson flow. As a result, the coupling of the plaquette shows similar behavior, as explained in the previous paragraph, while the other 7 couplings rapidly grow with increasing flow time. We discuss how this time evolution is interpreted from the point of view of the RG.

The rest of our paper is organized as follows. First, we define the exact differential equation for the effective action and show its solution in a truncated theory space in Sect. 2. Then we extend the equation to the gradient flow with arbitrary t-dependent action in Sect. 3. The case where S_t itself is chosen as a concrete example of the t-dependent action is considered in Sect. 3.2. We discuss similarities and differences of the time evolution compared to the Wilsonian RG flow in Sect. 3.3. A summary is given in Sect. 4.

2. Exact differential equation for the effective action

In this section, we derive the exact differential equation for the action starting from the Wilson flow equation for the link variables. The basic idea for the derivation has been proposed in the context of the exact renormalization group equation [17,18]. In this work, we concentrate on the 4D lattice $SU(3)$ pure Yang–Mills theory, but it is expected to be applied to various field theories. We also give a solution of the obtained equation in truncated 8-coupling theory space.

2.1. The effective action and its differential equation

Let us define the effective action S_t by the change of variables:

$$e^{-S_t[V]} \equiv \int DU\, \delta(V - \bar{V}_t[U])\, e^{-S_{\mathrm{W}}[U]}, \tag{2}$$

where $S_{\mathrm{W}}[U]$ is the Wilson plaquette action,

$$\begin{aligned} S_{\mathrm{W}}[U] &= -\frac{1}{6}\beta \sum_{x,\mu\neq\nu} \mathrm{Tr}\, W_{\mu\nu}(x) + \text{const.}, \quad \beta = 6/g_0^2, \\ W_{\mu\nu}(x) &= U_\mu(x)U_\nu(x+\mu)U_\mu^\dagger(x+\nu)U_\nu^\dagger(x), \end{aligned} \tag{3}$$

and $\bar{V}_t[U] = \{\bar{V}_\mu(x;t)\}$ is the solution of the Wilson flow equation,

$$\begin{aligned} \frac{d\bar{V}_\mu(x;t)}{dt} &= -g_0^2 \{\partial_{x,\mu} S_{\mathrm{W}}[U]\}|_{U=\bar{V}_t} \bar{V}_\mu(x;t), \\ \bar{V}_\mu(x;t)|_{t=0} &= U_\mu(x). \end{aligned} \tag{4}$$

Here we take t to be a dimensionless parameter. The differentiation with respect to the link variables on a differentiable function $f[U]$ is defined by

$$\begin{aligned} \partial^a_{x,\mu} f[U] &= \frac{d}{ds} f[U^s]\bigg|_{s=0}, \\ U^s_\nu(y) &= \begin{cases} e^{sT^a} U_\mu(x) & \text{if } (y,\nu) = (x,\mu), \\ U_\nu(y) & \text{otherwise,} \end{cases} \end{aligned} \tag{5}$$

and $\partial_{x,\mu} = T^a \partial^a_{x,\mu}$, where T^a are the anti-Hermitian $SU(3)$ generators whose normalization is given by

$$\mathrm{Tr}\,(T^a T^b) = -\frac{1}{2}\delta^{ab}. \tag{6}$$

With Eqs. (5) and (6), an infinitesimal change of $f[U]$ is

$$df[U] = -2 \sum_{x,\mu} \mathrm{Tr}\,[dU_\mu(x) U_\mu^{-1}(x) T^a]\, \partial^a_{x,\mu} f[U]. \tag{7}$$

To derive the differential equation for S_t, we differentiate both sides of Eq. (2) with respect to t:

$$-\frac{dS_t[V]}{dt}e^{-S_t[V]} = \int DU \frac{d}{dt}[\delta(V - \bar{V}_t[U])]\, e^{-S_{\mathrm{W}}[U]}. \tag{8}$$

The differentiation of the delta function in Eq. (8) is evaluated as

$$\frac{d}{dt}\delta(V - \bar{V}_t[U]) = g_0^2 \sum_{x,\mu} \bar{\partial}^a_{x,\mu} S_{\mathrm{W}}[\bar{V}_t]\, \partial^a_{x,\mu}[\delta(V - \bar{V}_t[U])], \tag{9}$$

where $\partial^a_{x,\mu}$ and $\bar{\partial}^a_{x,\mu}$ denote the differentiation with respect to $V_\mu(x)$ and $\bar{V}_\mu(x;t)$, respectively. Substituting Eq. (9) for Eq. (8), we finally obtain

$$-\frac{dS_t[V]}{dt}e^{-S_t[V]} = g_0^2 \sum_{x,\mu} \partial^a_{x,\mu}\left[\partial^a_{x,\mu} S_{\mathrm{W}}[V] e^{-S_t[V]}\right], \tag{10}$$

or, equivalently,

$$\frac{dS_t[V]}{dt} = g_0^2 \sum_{x,\mu} \{\partial^a_{x,\mu} S_t[V] \partial^a_{x,\mu} S_{\mathrm{W}}[V] - (\partial^a_{x,\mu})^2 S_{\mathrm{W}}[V]\}. \tag{11}$$

Note that this equation is independent of g_0^2 since $S_{\mathrm{W}} \propto 1/g_0^2$ and the overall g_0^2 on the right-hand side of Eq. (11) is canceled.

2.2. Solution in truncated theory space

We demonstrate computing S_t by solving Eq. (11) in this subsection. To this end, we truncate S_t, as is often the case in studies of a functional renormalization group. Note that this truncation is just for a practical reason and Eq. (11) itself is exact without any truncation. In the following, we take the truncation so that S_t is in the 8-coupling theory space:

$$S_t[V] = -\frac{1}{6}\sum_{i=0}^{7} \beta_i(t)\mathcal{W}_i[V] + (\text{independent of } V), \tag{12}$$

where each $\mathcal{W}_i$ is defined by the sum of the trace of the associated Wilson loops over the whole lattice:

$$\mathcal{W}_i = \sum_{C\in\mathcal{C}_i} \mathrm{Tr}\,\{U(C)\} \;\text{ if } i = 0,1,2,5,$$
$$\mathcal{W}_i = \sum_{\{C,C'\}\in\mathcal{C}_i} \mathrm{Tr}\,\{U(C)\}\mathrm{Tr}\,\{U(C')\} \;\text{ if } i = 3,4,6,7. \tag{13}$$

Here $U(C)$ denotes the the ordered product of the link variables along the loop C. The Wilson plaquette is associated with $\mathcal{C}_0$. The other classes $\mathcal{C}_{i\geq 1}$ of Wilson loops and pairs of them are constructed by the contraction of two Wilson plaquettes with a common link variable (see Fig. 1). There are some missing length-6 operators (see, e.g., Fig. 2). However, three Wilson plaquettes are needed to make such operators, which are subleading in powers of t. Solving the gradient flow equation is regarded as continuously contracting operators with a Wilson plaquette. Therefore, an operator that requires a smaller number of Wilson plaquettes makes the contributions in smaller powers of t. Hereafter we

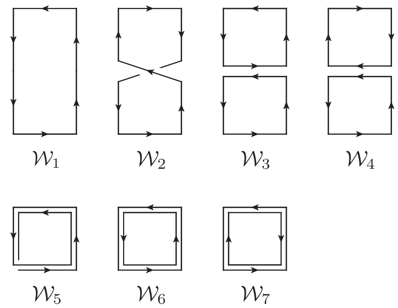

Fig. 1. Classes of Wilson loops and pairs of them in the truncated S_t. The loops 5, 6, 7 lie on a single plaquette of the lattice. The other loops occupy two plaquettes that can lie in a plane or be at right angles in three dimensions.

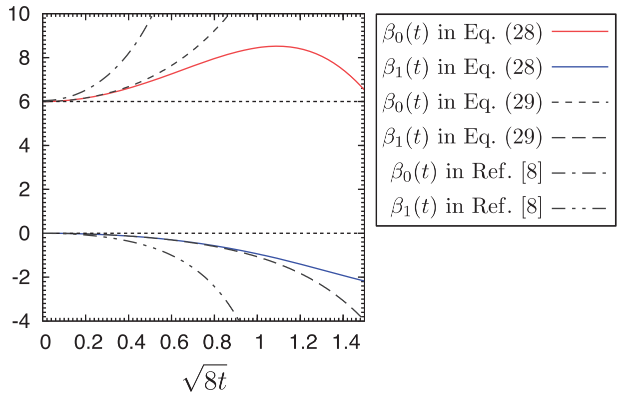

Fig. 2. A missing length-6 operator.

omit the V-independent term in S_t. We also take the initial condition as $S_0 = S_{\mathrm{W}}$, specifically,

$$\beta_0(0) = \beta, \qquad \beta_i(0) = 0 \ \text{ if } i = 1, \ldots, 7, \tag{14}$$

for simplicity.

Note that the truncation is reasonable in the small-t regime, since contributions from the loops that occupy a larger area of the lattice are not negligible in a large-t regime. In fact, the solution under the above truncation scheme is the same as the exact one up to $O(t^2)$. For higher orders in t, the number of Wilson loops required grows factorially and analytic calculation becomes harder. The correctness of the effective action can be checked by verifying that the observables at flow time t correspond to those computed with S_t.

Now let us rewrite Eq. (11) as differential equations for $\beta_i(t)$. The left-hand side of Eq. (11) becomes

$$\frac{dS_t[V]}{dt} = -\frac{1}{6}\sum_{i=0}^{7}\frac{d\beta_i(t)}{dt}\mathcal{W}_i[V], \tag{15}$$

where the differentiation is performed at constant V.

To compute the right-hand side of Eq. (11), we make use of an identity for the $SU(3)$ generators:

$$(T^a)_{\alpha\beta}(T^a)_{\gamma\delta} = -\frac{1}{2}\left(\delta_{\alpha\delta}\delta_{\beta\gamma} - \frac{1}{3}\delta_{\alpha\beta}\delta_{\gamma\delta}\right). \tag{16}$$

Some algebraic manipulations yield

$$\sum_{x,\mu} \partial^a_{x,\mu} \mathcal{W}_0 \, \partial^a_{x,\mu} \mathcal{W}_0 = \mathcal{W}_1 - \mathcal{W}_2 - \tfrac{1}{3}\mathcal{W}_3 + \tfrac{1}{3}\mathcal{W}_4 - 2\mathcal{W}_5 + \tfrac{2}{3}\mathcal{W}_6 - \tfrac{4}{3}\mathcal{W}_7, \tag{17}$$

$$\sum_{x,\mu} \partial^a_{x,\mu} \mathcal{W}_1 \, \partial^a_{x,\mu} \mathcal{W}_0 = 30\mathcal{W}_0 + \cdots, \tag{18}$$

$$\sum_{x,\mu} \partial^a_{x,\mu} \mathcal{W}_2 \, \partial^a_{x,\mu} \mathcal{W}_0 = 50\mathcal{W}_0 + \cdots, \tag{19}$$

$$\sum_{x,\mu} \partial^a_{x,\mu} \mathcal{W}_3 \, \partial^a_{x,\mu} \mathcal{W}_0 = 120\mathcal{W}_0 + \cdots, \tag{20}$$

$$\sum_{x,\mu} \partial^a_{x,\mu} \mathcal{W}_4 \, \partial^a_{x,\mu} \mathcal{W}_0 = 120\mathcal{W}_0 + \cdots, \tag{21}$$

$$\sum_{x,\mu} \partial^a_{x,\mu} \mathcal{W}_5 \, \partial^a_{x,\mu} \mathcal{W}_0 = 4\mathcal{W}_0 + \cdots, \tag{22}$$

$$\sum_{x,\mu} \partial^a_{x,\mu} \mathcal{W}_6 \, \partial^a_{x,\mu} \mathcal{W}_0 = 12\mathcal{W}_0 + \cdots, \tag{23}$$

$$\sum_{x,\mu} \partial^a_{x,\mu} \mathcal{W}_7 \, \partial^a_{x,\mu} \mathcal{W}_0 = 6\mathcal{W}_0 + \cdots, \tag{24}$$

$$\sum_{x,\mu} (\partial^a_{x,\mu})^2 \mathcal{W}_0 = -\tfrac{16}{3}\mathcal{W}_0, \tag{25}$$

up to an irrelevant constant in V. The omitted part in Eqs. (18)–(24) does not contain $\mathcal{W}_{1\leq i\leq 7}$.

Comparing the coefficients of $\mathcal{W}_i$ on both sides of Eq. (11), we finally obtain

$$\frac{d\beta_i(t)}{dt} = \sum_{j=0}^{7} M_{ij}\beta_j(t) + 32\delta_{i0}, \tag{26}$$

where M_{ij} is the 8×8 real matrix given by

$$M_{ij} = \begin{pmatrix} 0 & -30 & -50 & -120 & -120 & -4 & -12 & -6 \\ -1 & 0 & 0 & 0 & 0 & 0 & 0 & 0 \\ 1 & 0 & 0 & 0 & 0 & 0 & 0 & 0 \\ \frac{1}{3} & 0 & 0 & 0 & 0 & 0 & 0 & 0 \\ -\frac{1}{3} & 0 & 0 & 0 & 0 & 0 & 0 & 0 \\ 2 & 0 & 0 & 0 & 0 & 0 & 0 & 0 \\ -\frac{2}{3} & 0 & 0 & 0 & 0 & 0 & 0 & 0 \\ \frac{4}{3} & 0 & 0 & 0 & 0 & 0 & 0 & 0 \end{pmatrix}, \tag{27}$$

within our truncation scheme. Note that, since the right-hand side of Eq. (11) is linear in S_t, the differential equation of $\beta_i(t)$ always forms as Eq. (26) with any truncation. Equation (26) is just a linear inhomogeneous first-order differential equation and is easily solved analytically.

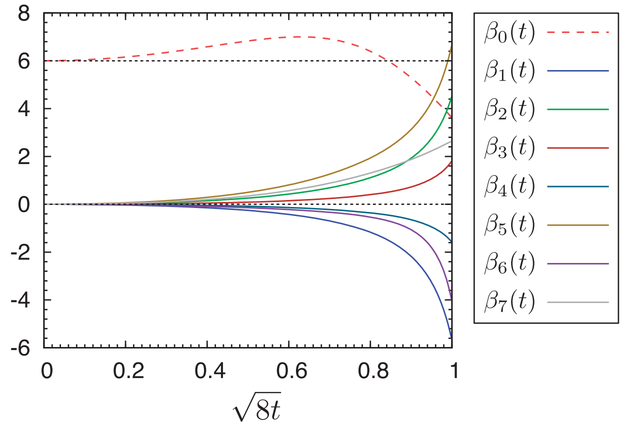

Fig. 3. $\beta_0(t)$ and $\beta_1(t)$ as functions of $\sqrt{8t}$. The value of β, which is the initial value of $\beta_0(t)$, is taken to be 6, the same as that in Ref. [8]. The solid lines represent $\beta_0(t)$ and $\beta_1(t) = -\gamma(t)$ in Eq. (28), the dashed lines represent those in Eq. (29), and the dot-dashed lines represent those determined in Ref. [8] by the lattice simulation.

The solutions of $\beta_i(t)$ with Eqs. (14) and (27) are given by

$$\begin{aligned}\beta_0(t) &= \beta \cos\left(2\sqrt{7}t\right) + \frac{16}{\sqrt{7}} \sin\left(2\sqrt{7}t\right),\\ \beta_i(t) &= M_{i0}\gamma(t), \quad \text{for} \ \ i = 1, \ldots, 7,\\ \gamma(t) &= \frac{8}{7}\left[1 - \cos\left(2\sqrt{7}t\right)\right] + \frac{\beta}{2\sqrt{7}} \sin\left(2\sqrt{7}t\right).\end{aligned} \tag{28}$$

We plot these solutions as functions of $\sqrt{8t}$ in Fig. 3. $\beta = 6$ is used for the initial condition. Note that $\beta_1(t) = M_{10}\gamma(t) = -\gamma(t)$ and $\beta_{i\geq 2}(t)$ are proportional to $\gamma(t)$. The two dot-dashed lines in Fig. 3 represent $\beta_0(t)$ and $\beta_1(t)$ obtained by the numerical fit in Ref. [8], where S_t is truncated so that it has Wilson plaquettes and rectangles only.

From Fig. 3, the two approaches agree on the negativeness of $\beta_1(t)$ at $t > 0$, which has already been reported in Ref. [8]; however, the flow-time dependence is clearly different. This can be understood as the difference of the truncation of S_t, since we obtain

$$\begin{aligned}\beta_0(t) &= \beta \cosh\left(\sqrt{30}t\right) + \frac{16\sqrt{30}}{15} \sinh\left(\sqrt{30}t\right),\\ \beta_1(t) &= -\frac{16}{15}\left[\cosh\left(\sqrt{30}t\right) - 1\right] - \frac{\sqrt{30}}{30}\beta \sinh\left(\sqrt{30}t\right),\end{aligned} \tag{29}$$

when we set $\beta_{i\geq 2}(t)$ to be 0 in Eq. (26). These solutions are plotted as two dashed lines in Fig. 3. A similar exponential dependence in t has been observed in Ref. [8], although the value of the exponent still does not coincide.

For our solution, the flow-time dependence of $\beta_0(t)$ looks interesting. Since the expectation value of the plaquette at finite t is considered to be larger than that of the plaquette at $t = 0$, we naively expect the coupling of the plaquette to increase monotonically with t. On the other hand, our result shows that it increases in the small-t region due to the second term on the right-hand side of Eq. (26), then starts to decrease at around $\sqrt{8t} \simeq 1$. This looks inconsistent with our naive guess. However, we may not discuss the value of the plaquette based only on $\beta_0(t)$ because the inverse of the squared "effective gauge coupling" is not given by $\beta_0(t)$ but by a suitable linear combination of $\beta_i(t)$. Algebraically, the second derivative of $\beta_0(t)$ with respect to t satisfies

$$\frac{d^2\beta_0(t)}{dt^2} = M_{00}^2\beta_0, \;\; M_{00}^2 = -28 < 0, \tag{30}$$

in this truncation, which causes such behavior of $\beta_0(t)$.

3. Extension to flow-time-dependent gradient flow

In this section, we consider the extension of Eq. (11) to more generic cases. Specifically, the flow equation is not limited to the Wilson flow equation (Eq. (4)) but can be taken as a flow equation with an arbitrary chosen action. For example, the "trivializing action" [2], which gives the vanishing S_t at a fixed $t = t_0$, could be a good candidate. S_t itself can also be chosen as the seeding action generating S_{t+dt}, similar to a conventional RG transformation.

3.1. *Extension of Eq.* (11)

To extend Eq. (11) to more generic cases, let us consider an infinitesimal change of the flow time at t as follows:

$$e^{-S_{t+dt}[V']} = \int DV \; \delta(V' - \bar{V}_{dt}[V]) \; e^{-S_t[V]}. \tag{31}$$

Suppose that $\bar{V}_{dt}[V]$ is given by

$$\bar{V}_\mu(x; dt)[V] = V_\mu(x) - \{\partial_{x,\mu}\mathcal{S}_t[V]\}V_\mu(x)dt + O((dt)^2), \tag{32}$$

where $\mathcal{S}_t[V]$ is an arbitrary t-dependent action generating the flow of the link variables from t to $t+dt$. Then, by comparing the $O(dt)$ terms on both sides of Eq. (31), we obtain the flow-time-dependent gradient flow equation for S_t:

$$\frac{dS_t[V]}{dt} = \sum_{x,\mu}\{\partial_{x,\mu}^a S_t[V]\partial_{x,\mu}^a \mathcal{S}_t[V] - (\partial_{x,\mu}^a)^2\mathcal{S}_t[V]\}, \tag{33}$$

where an initial action can be any lattice action that consists of Wilson loops and products of them. When we choose $\mathcal{S}_t = g_0^2 S_{\mathrm{W}}$, Eq. (33) is equivalent to Eq. (11), in which the flow of S_t is generated by the Wilson flow.

3.2. *A concrete example:* $\mathcal{S}_t = g_0^2 S_t$

In this subsection, we analyze Eq. (33) in the case of $\mathcal{S}_t = g_0^2 S_t$, namely,

$$\frac{dS_t[V]}{dt} = g_0^2\sum_{x,\mu}\{\partial_{x,\mu}^a S_t[V]\partial_{x,\mu}^a S_t[V] - (\partial_{x,\mu}^a)^2 S_t[V]\}, \tag{34}$$

with the same truncation (Eq. (12) and Fig. 1) and initial condition (Eq. (14)) of S_t as in Sect. 2.2.

The computation is almost the same as in the previous section. For this case, we additionally need the relations in Appendix A in order to derive the following differential equation for $\beta_i(t)$:

$$\frac{d\beta_0(t)}{dt} = -\frac{\beta_0(t)}{\beta}[60\beta_1(t) + 100\beta_2(t) + 240\beta_3(t) + 240\beta_4(t) + 8\beta_5(t) + 24\beta_6(t) + 12\beta_7(t) - 32], \tag{35}$$

$$\frac{d\beta_1(t)}{dt} = -\frac{1}{\beta}\left[\beta_0^2(t) + 12\beta_1^2(t) + 28\beta_2^2(t) + 20\beta_2(t)\beta_5(t) - 48\beta_1(t) + 6\beta_3(t)\right], \tag{36}$$

$$\frac{d\beta_2(t)}{dt} = -\frac{1}{\beta}\left[-\beta_0^2(t) + 24\beta_1(t)\beta_2(t) + 12\beta_1(t)\beta_5(t) - 62\beta_2(t) - 6\beta_4(t)\right], \tag{37}$$

$$\begin{aligned}\frac{d\beta_3(t)}{dt} = -\frac{1}{\beta}\Big[&-\tfrac{1}{3}\beta_0^2(t) + 24\beta_1(t)\beta_3(t) + 6\beta_1(t)\beta_7(t) + 40\beta_2(t)\beta_4(t) + 20\beta_2(t)\beta_6(t)\\ &+ 48\beta_3^2(t) + 24\beta_3(t)\beta_7(t) + 48\beta_4^2(t) + 16\beta_4(t)\beta_5(t) + 48\beta_4(t)\beta_6(t)\\ &- 66\beta_3(t)\Big],\end{aligned} \tag{38}$$

$$\begin{aligned}\frac{d\beta_4(t)}{dt} = -\frac{1}{\beta}\Big[&\tfrac{1}{3}\beta_0^2(t) + 24\beta_1(t)\beta_4(t) + 12\beta_1(t)\beta_6(t) + 40\beta_2(t)\beta_3(t) + 10\beta_2(t)\beta_7(t)\\ &+ 96\beta_3(t)\beta_4(t) + 16\beta_3(t)\beta_5(t) + 48\beta_3(t)\beta_6(t) + 24\beta_4(t)\beta_7(t) - 6\beta_2(t)\\ &-62\beta_4(t)\Big],\end{aligned} \tag{39}$$

$$\frac{d\beta_5(t)}{dt} = -\frac{1}{\beta}\left[-2\beta_0^2(t) + 60\beta_1(t)\beta_2(t) - 56\beta_5(t) - 24\beta_6(t)\right], \tag{40}$$

$$\begin{aligned}\frac{d\beta_6(t)}{dt} = -\frac{1}{\beta}\Big[&\tfrac{2}{3}\beta_0^2(t) + 60\beta_1(t)\beta_4(t) + 60\beta_1(t)\beta_6(t) + 100\beta_2(t)\beta_3(t) + 240\beta_3(t)\beta_4(t)\\ &+ 8\beta_5(t)\beta_7(t) + 24\beta_6(t)\beta_7(t) - 24\beta_5(t) - 56\beta_6(t)\Big],\end{aligned} \tag{41}$$

$$\begin{aligned}\frac{d\beta_7(t)}{dt} = -\frac{1}{\beta}\Big[&-\tfrac{4}{3}\beta_0^2(t) + 60\beta_1(t)\beta_3(t) + 100\beta_2(t)\beta_4(t) + 240\beta_3^2(t) + 240\beta_4^2(t)\\ &+ 32\beta_5(t)\beta_6(t) + 48\beta_6^2(t) + 12\beta_7^2(t) - 72\beta_7(t)\Big],\end{aligned} \tag{42}$$

within our truncation scheme. These are no longer solved analytically since the equations are quadratic in $\beta_i(t)$, which is the consequence of the fact that Eq. (34) is quadratic in S_t.

As in Sect. 2.2, the numerical solutions of Eqs. (35)–(42) with $\beta = 6$ are plotted in Fig. 4 as functions of $\sqrt{8t}$. The dashed line represents $\beta_0(t)$ and the solid lines represent $\beta_{i\geq 1}(t)$. Figure 4 shows that the behavior of $\beta_0(t)$ is similar to that in Sect. 2.2, while $|\beta_{i\geq 1}(t)|$ rapidly grows with increasing t. Comparing Eqs. (35)–(42) with Eq. (26), we have linear and quadratic terms in $\beta_{i\geq 1}(t)$ on the right-hand sides of Eqs. (36)–(42), which amplify the value of $|\beta_{i\geq 1}(t)|$. Then $\beta_0(t)$ receives the effect of this growth in $|\beta_{i\geq 1}(t)|$ and decreases to less than its initial value. These points explain the interesting time evolution of the couplings shown in Fig. 4.

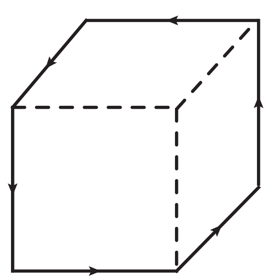

Fig. 4. Numerical solutions of $\beta_i(t)$ as functions of $\sqrt{8t}$ with $\beta = 6$, as in Fig. 3. The dashed line represents $\beta_0(t)$ and the solid lines represent $\beta_{i\geq 1}(t)$.

3.3. Similarities and differences compared to the Wilsonian RG flow

As noted in Sect. 1, we want to reveal the deeper connection between the gradient flow and the Wilsonian RG. Here we discuss this subject based on the result in Sect. 3.2.

First, we note how Eq. (34) looks similar to the RG equation. In the Wilsonian RG, we start with a Wilsonian effective action S_Λ at a given cutoff Λ. We integrate out the shell mode of S_Λ, then obtain $S_{\Lambda-d\Lambda}$. Namely, $S_{\Lambda-d\Lambda}$ is calculated by using S_Λ. By analogy with this fact, the use of S_t as the seeding action makes the differential equation more similar to the exact RG equation, if we identify the flow time as a cutoff scale (in position space). Moreover, in Ref. [19], Polchinski's RG equation is shown as Eq. (3.30), where S^I is an interaction part of the Wilsonian effective action and $\dot{C}$ corresponds to the exact RG kernel. When we regard $-\Lambda\partial_\Lambda$ as d/dt, S^I as S_t, $\delta/\delta\phi$ as $\partial_{x,\mu}$, and $\dot{C}/2$ as a constant, Eq. (3.30) in Ref. [19] looks like (34).

Next we discuss the obtained flow of the couplings. Let us assume that the flow-time dependence of $\beta_0(t)$ described in Sect. 3.2 is common to any $\beta_i(t)$: we assume that the absolute value of a coupling $\beta_i(t)$ associated with a class of operators whose "extent" is n becomes large at $(n-1) \lesssim \sqrt{8t} \lesssim n$ and small at $\sqrt{8t} \gtrsim n$. The word "extent" roughly means how many plaquette the operator occupies. This implies that Eq. (34) contains a picture of the renormalization group, in which short-distance interactions disappear in the action. When we increase the flow time, operators of the "extent" $= n$ disappear while those of the "extent" $= n+1$ appear; this process should repeat. To confirm the above statement, a truncated theory space should be enlarged while the number of conceivable classes of Wilson loops increases factorially. The simplest way is to add the class of operators constructed by contracting three Wilson plaquettes.

However, since the gradient flow is just a smearing of the link variables, the time evolution of S_t does not have a coarse-graining step. S_t is defined on the fine lattice even in the large-t regime. Therefore, we need a coarse-graining step to eventually construct an RG scheme in this approach, e.g., to obtain the beta function of the gauge coupling. Once the absolute value of couplings becomes sufficiently small, we can throw away the operators associated with such couplings, which would give the coarse-graining step. However, we do not know how this procedure would be implemented systematically and quantitatively at this point. Therefore, this could be part of our future work. Note that a coarse-graining step on the lattice could define a discretized RG equation rather than a continuous (differential) one like Eq. (33).

4. Summary

In this work, we have first proposed the exact differential equation for the effective action S_t defined by Eq. (2), which enables us to determine the flow-time dependence of the action without lattice simulations. It is investigated in truncated 8-coupling theory space (Eq. (12) and Fig. 1) and analytical solutions have been obtained (Eq. (28)). Then the equation is extended to more generic cases, where the flow equation of link variables is not limited to the Wilson flow but can be a gradient flow with an arbitrary t-dependent action $\mathcal{S}_t$. We have also analyzed a concrete example of it, $\mathcal{S}_t = g_0^2 S_t$, in Sect. 3.2 and given the solution in the same truncated theory space as the case of the Wilson flow.

For the case of the Wilson flow, the differential equation of couplings becomes a linear inhomogeneous first-order differential equation with any truncation; therefore, it can be solved analytically. The solutions are shown in Eq. (28) and plotted in Fig. 3 as functions of $\sqrt{8t}$. We have found that the coefficient of the rectangle (β_1) tends to be negative at $t > 0$, which agrees with the result of Ref. [8] and known improved actions [11–16]. However, the flow-time dependence of couplings is different from that of Ref. [8]. For our solution, the coefficient of the Wilson plaquette (β_0) increases at the beginning, then starts to decrease at around $\sqrt{8t} \simeq 1$.

For the case of $\mathcal{S}_t = g_0^2 S_t$, the differential equation of couplings is no longer integrated analytically, since it is quadratic in couplings. The numerical solutions are shown in Fig. 4, the same as the case of the Wilson flow. Similarly to the case of the Wilson flow, $\beta_0(t)$ increases at the beginning then decreases to less than its initial value. On the other hand, $|\beta_{i\geq 1}(t)|$ seems to rapidly increase with flow time. These results are caused by linear and quadratic terms in $\beta_{i\geq 1}(t)$ on the right-hand sides of Eqs. (35)–(42), which are absent in Eq. (26). We then discussed the possibility of regarding this time evolution as the Wilsonian RG flow. To complete our final goal of constructing the gauge-invariant RG from the gradient flow, we need to make the differential equation contain a coarse-graining step.

Finally, we comment on our truncation of the effective action. The Wilson plaquette and 7 classes of Wilson loops and their products (Fig. 1), which can be constructed by contracting two Wilson plaquettes with a common link variable, have been taken into account in this work. This truncation is only compatible with the small-flow-time expansion for the case of the Wilson flow in Sect. 2. Hence, the solution of Eq. (11) is exact up to $O(t^n)$ when all of the classes contracting up to n Wilson plaquettes are included in S_t. On the other hand, for the case of $\mathcal{S}_t = g_0^2 S_t$ in Sect. 3.2, we should include other loops in S_t if we want an accurate solution in the small-flow-time expansion.

Acknowledgements

I would like to express my deepest gratitude to Kengo Kikuchi for giving me a chance to consider this work. I also thank Hidenori Fukaya and Tetsuya Onogi for fruitful discussions and careful reading of this manuscript, and Akio Tomiya for useful comments. This work is supported in part by a Grand-in-Aid of the Japanese Ministry of Education No. 15J01081.

Appendix. Calculation details for the derivation of Eqs. (35)–(42)

To evaluate the first term on the right-hand side of Eq. (34), we need to compute the coefficient $T_{ij,k}$ $(i, j, k = 1, \ldots, 7)$ defined by

$$\sum_{x,\mu} \partial^a_{x,\mu} \mathcal{W}_i \partial^a_{x,\mu} \mathcal{W}_j = \sum_{k=0}^{7} T_{ij,k} \mathcal{W}_k + \cdots , \tag{A1}$$

in addition to Eqs. (17)–(24). By this definition, $T_{ij,k}$ is symmetric in the exchange between i and j: $T_{ij,k} = T_{ji,k}$. We list nonzero elements of $T_{ij,k}$ in the following:

$$\begin{aligned}
&T_{11,1} = 12, && T_{22,1} = 28, && T_{25,1} = 20, && T_{12,2} = 24,\\
&T_{15,2} = 12, && T_{13,3} = 24, && T_{17,3} = 6, && T_{24,3} = 40,\\
&T_{26,3} = 20, && T_{33,3} = 48, && T_{37,3} = 24, && T_{44,3} = 48,\\
&T_{45,3} = 16, && T_{46,3} = 48, && T_{14,4} = 24, && T_{16,4} = 12,\\
&T_{23,4} = 40, && T_{27,4} = 10, && T_{34,4} = 96, && T_{35,4} = 16,\\
&T_{36,4} = 48, && T_{47,4} = 24, && T_{12,5} = 60, && T_{14,6} = 60,\\
&T_{16,6} = 60, && T_{23,6} = 100, && T_{34,6} = 240, && T_{57,6} = 8,\\
&T_{67,6} = 24, && T_{13,7} = 60, && T_{24,7} = 100, && T_{33,7} = 240,\\
&T_{44,7} = 240, && T_{56,7} = 32, && T_{66,7} = 48, && T_{77,7} = 12.
\end{aligned} \tag{A2}$$

For the second term, the following relations are needed in addition to Eq. (25):

$$\sum_{x,\mu} (\partial^a_{x,\mu})^2 \mathcal{W}_1 = -8\mathcal{W}_1, \tag{A3}$$

$$\sum_{x,\mu}(\partial^a_{x,\mu})^2\mathcal{W}_2 = -\tfrac{31}{3}\mathcal{W}_2 - \mathcal{W}_4, \tag{A4}$$

$$\sum_{x,\mu}(\partial^a_{x,\mu})^2\mathcal{W}_3 = -11\mathcal{W}_3 + \mathcal{W}_1, \tag{A5}$$

$$\sum_{x,\mu}(\partial^a_{x,\mu})^2\mathcal{W}_4 = -\tfrac{31}{3}\mathcal{W}_4 - \mathcal{W}_2, \tag{A6}$$

$$\sum_{x,\mu}(\partial^a_{x,\mu})^2\mathcal{W}_5 = -\tfrac{28}{3}\mathcal{W}_5 - 4\mathcal{W}_6, \tag{A7}$$

$$\sum_{x,\mu}(\partial^a_{x,\mu})^2\mathcal{W}_6 = -\tfrac{28}{3}\mathcal{W}_6 - 4\mathcal{W}_5, \tag{A8}$$

$$\sum_{x,\mu}(\partial^a_{x,\mu})^2\mathcal{W}_7 = -12\mathcal{W}_7 + (\text{independent of } V). \tag{A9}$$

References

[1] R. Narayanan and H. Neuberger, J. High Energy Phys. **03**, 064 (2006) [arXiv:hep-th/0601210] [Search INSPIRE].

[2] M. Lüscher, Commun. Math. Phys. **293**, 899 (2010) [arXiv:0907.5491 [hep-lat]] [Search INSPIRE].

[3] M. Lüscher, J. High Energy Phys. **08**, 071 (2010); **03**, 092 (2014) [erratum] [arXiv:1006.4518 [hep-lat]] [Search INSPIRE].

[4] M. Lüscher, PoS **LATTICE2013**, 016 (2014) [arXiv:1308.5598 [hep-lat]] [Search INSPIRE].

[5] M. Lüscher and P. Weisz, J. High Energy Phys. **02**, 051 (2011) [arXiv:1101.0963 [hep-th]] [Search INSPIRE].

[6] H. Makino and H. Suzuki, Prog. Theor. Exp. Phys. **2015**, 033B08 (2015) [arXiv:1410.7538 [hep-lat]] [Search INSPIRE].

[7] S. Aoki, K. Kikuchi, and T. Onogi, J. High Energy Phys. **04**, 156 (2015) [arXiv:1412.8249 [hep-th]] [Search INSPIRE].

[8] A. Kagimura, A. Tomiya, and R. Yamamura, arXiv:1508.04986 [hep-lat] [Search INSPIRE].

[9] M. Creutz, Phys. Rev. Lett. **50**, 1411 (1983).

[10] M. Hasenbusch, K. Pinn, and C. Wieczerkowski, Phys. Lett. B **338**, 308 (1994) [arXiv:hep-lat/9406019] [Search INSPIRE].

[11] P. Weisz, Nucl. Phys. B **212**, 1 (1983).

[12] P. Weisz and R. Wohlert, Nucl. Phys. B **236**, 397 (1984); **247**, 544 (1984) [erratum].

[13] M. Lüscher and P. Weisz, Commun. Math. Phys. **97**, 59 (1985); **98**, 433 (1985) [erratum].

[14] Y. Iwasaki, arXiv:1111.7054 [hep-lat] [Search INSPIRE].

[15] Y. Iwasaki, Nucl. Phys. B **258**, 141 (1985).

[16] P. de Forcrand, M. Garcia Perez, T. Hashimoto, S. Hioki, H. Matsufuru, O. Miyamura, A. Nakamura, I. O. Stamatescu, T. Takaishi, and T. Umeda, Nucl. Phys. B **577**, 263 (2000) [arXiv:hep-lat/9911033] [Search INSPIRE].

[17] F. J. Wegner, J. Phys. C **7**, 2098 (1974).

[18] J. I. Latorre and T. R. Morris, J. High Energy Phys. **11**, 004 (2000) [arXiv:hep-th/0008123] [Search INSPIRE].

[19] O. J. Rosten, Phys. Rept. **511**, 177 (2012) [arXiv:1003.1366 [hep-th]] [Search INSPIRE].